CrossMark

Experimental Investigation and Thermodynamic Calculation of the Phase Equilibria in the Cu-Nb-Zr Ternary System

X.J. Liu, Y. Liu, Y.H. Guo, D. Wang, S.Y. Yang, Y. Lu, and C.P. Wang

The phase equilibria of the Cu-Nb-Zr ternary system at 900, 1000 and 1100 °C were experimentally investigated by optical microscopy and electron probe microanalysis on the equilibrated alloys. Combined with the obtained experimental results, the phase equilibria of Cu-Nb-Zr ternary system were thermodynamically optimized using the CALPHAD (calculation of phase diagrams) method. The Gibbs free energies of the phases in the present work were described by appropriate models. A consistent set of the thermodynamic parameters leading to reasonable agreement between the calculated data and experimental results was obtained in the Cu-Nb-Zr ternary system.

1. Introduction

Cu-Nb-based conductors exhibit extremely high strength along good conductivity, which are considered to be used in windings of high field pulsed magnets.[1-3] Popva et al. reported that doping with Zr in the Cu-Nb alloys would increase ultimate tensile strength and microhardness of the materials.[4] However, there is still no comprehensive understanding of microstructural evolution, which makes it difficult to attain further improvement of these materials. Specially, it is not clear about the appropriate Zr content that influences the structure and properties. Thus, more information concerning the phase equilibria in the Cu-Nb-Zr ternary phase diagram is necessary. Up to now, Frolova et al. studied the structure and superconducting properties of a Nb-33% alloy containing Cu in 1967.[5] Kudryavisev et al. investigated the Zr corner of Cu-Nb-Zr phase diagram in 1968.[6] However, no systematic information is reported in the Cu-Nb-Zr ternary system in the relevant literature. Therefore, in order to obtain accurate information concerning the phase equilibria in the Cu-Nb-Zr ternary phase diagram, the precise investigations of the phase equilibria by

both experiment and thermodynamic assessment are necessary.

The information of the binary subsystems in the Cu-Nb-Zr ternary system is completely determined by experiments[7-19] and thermodynamic assessment. The three calculated binary phase diagrams of the Cu-Nb,[20] Nb-Zr[21] and Cu-Zr[22] are used in the present work, as shown in Fig. 1. Only three phases, i.e. liquid, (Cu) and (Nb) are involved in the Cu-Nb system. The Cu-Nb phase diagram is of the peritectic type with limited solubility, whether the matrix is Cu or Nb. In addition, the metastable $L_1 + L_2$ phase is shown with dashed line in the diagram. For Nb-Zr phase diagram, there are no intermediate phases in this system. The bcc β-Nb and β-Zr form a continuous solid solution (βZr,βNb) at high temperature. Meanwhile, there is a spinodal decomposition of BCC in the Nb-Zr system. The binary Cu-Zr system was assessed by Gierlotka,[22] where twelve phases are contained: αZr (low temperature Zr), βZr (high temperature Zr), FCC_A1(Cu), intermetallic compounds Cu_9Zr_2, $Cu_{51}Zr_{14}$, Cu_8Zr_3, Cu_2Zr, $Cu_{10}Zr_7$, CuZr, Cu_5Zr_7 $CuZr_2$ and liquid.

The objective of the present work is to experimentally investigate the phase equilibria in the Cu-Nb-Zr ternary systems at 900, 1000 and 1100 °C. Then based on the experimental results, the thermodynamic calculation of the phase equilibria in the Cu-Nb-Zr system is studied by means of the CALPHAD method.[23-25] The results obtained in the present work are expected to give a better understanding of the microstructure in the Cu-Nb-Zr alloys for its practical applications.

X.J. Liu, S.Y. Yang, Y. Lu, and **C.P. Wang**, Department of Materials Science and Engineering, College of Materials, Xiamen University, Xiamen 361005, People's Republic of China; and Research Center of Materials Design and Applications, Xiamen University, Xiamen 361005, People's Republic of China; and **Y. Liu, Y.H. Guo,** and **D. Wang,** Department of Materials Science and Engineering, College of Materials, Xiamen University, Xiamen 361005, People's Republic of China. Contact e-mails: lxj@xmu.edu.cn and wangcp@xmu.edu.cn.
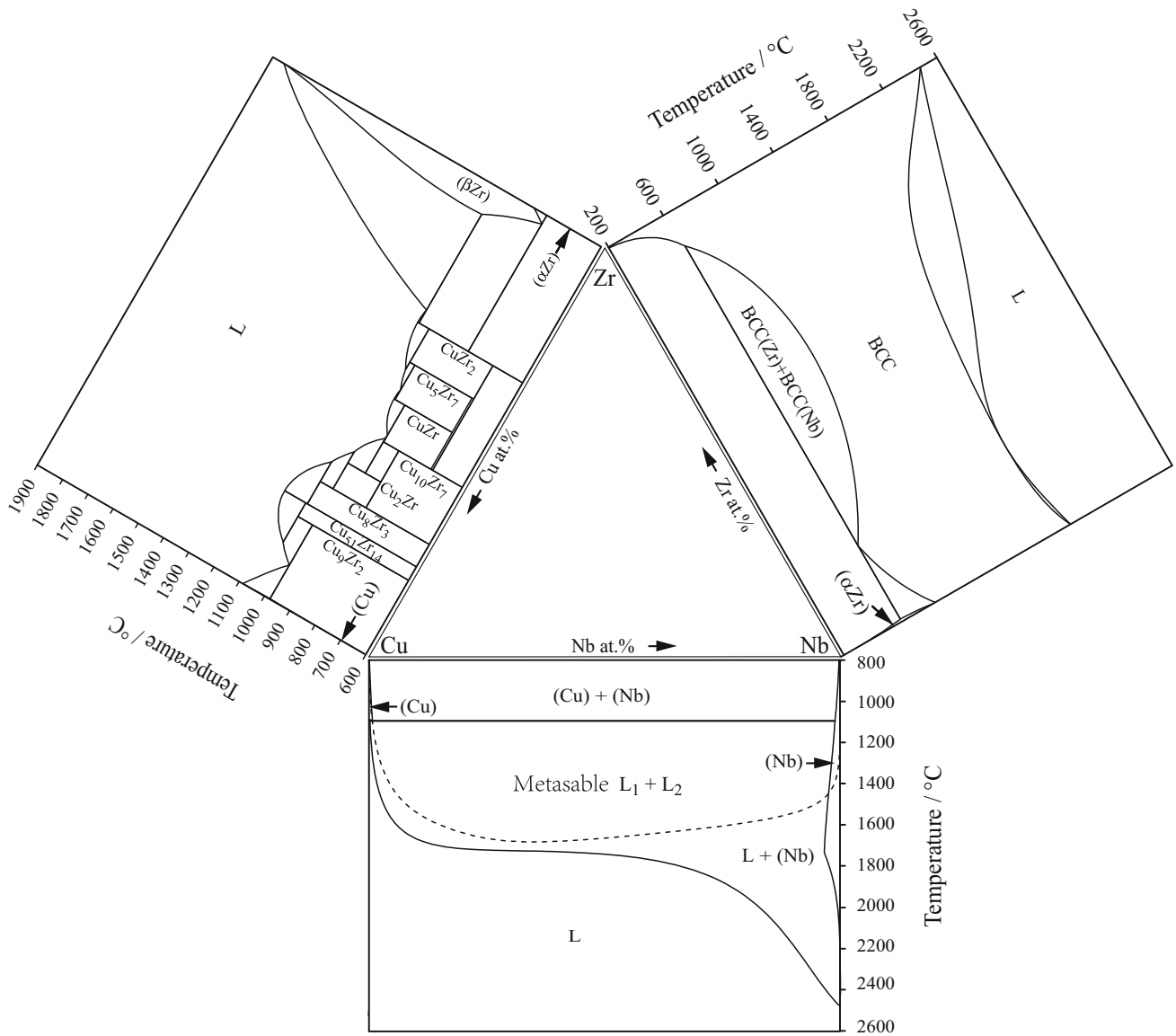
2. Experimental Procedure

Copper (99.9 wt.%), niobium(99.9 wt.%) and zirconium (99.9 wt.%) were used as starting materials. Bulk buttons were prepared from pure elements by arc melting under an

Fig. 1 Calculated binary phase diagrams constituting the Cu-Nb-Zr ternary system

argon atmosphere and in a water-cooled copper crucible. In order to ensure compositional uniformity, the ingots about 15 g were arc-melted at least five times. Prior to heat treatment, the specimens were sealed in quartz capsules in a high purity argon atmosphere.

The specimens were annealed at 900, 1000 and 1100 °C, respectively. The time of heat treatment varied from several hours to several days depending on the annealing temperature and the specimen composition. At the end of the heat treatment, the specimens were taken out of the furnace and quenched into ice water.

After annealing and standard metallographic preparation, the micro-structural observations were carried out by optical microscopy. Then the equilibrium compositions of the phases were measured by EPMA (JXA-8100R, JEOL, Japan). Pure elements were used as standards and the

measurements were carried out at 20.0 kV. EDS was used to determine the composition of the liquid phase.

3. Experimental Results and Discussion

3.1 Microstructure and Phase Equilibria

In this work, each phase is identified by the equilibrium composition measured by EPMA. BSE (back-scattered electron) images of typical ternary Cu-Nb-Zr alloys are illustrated in Fig. 2(a) to (f). Figure 2(a) shows the three-phase microstructure (Cu_9Zr_2 + (Cu) + BCC(Nb)) of the $Cu_{60}Nb_{30}Zr_{10}$ (Here-after, alloy compositions are indicated in at.%) alloy annealed at 900 °C for 38 days. The three-phase microstructure (Cu_8Zr_3 + $CuZr_2$ + BCC(Nb)) was
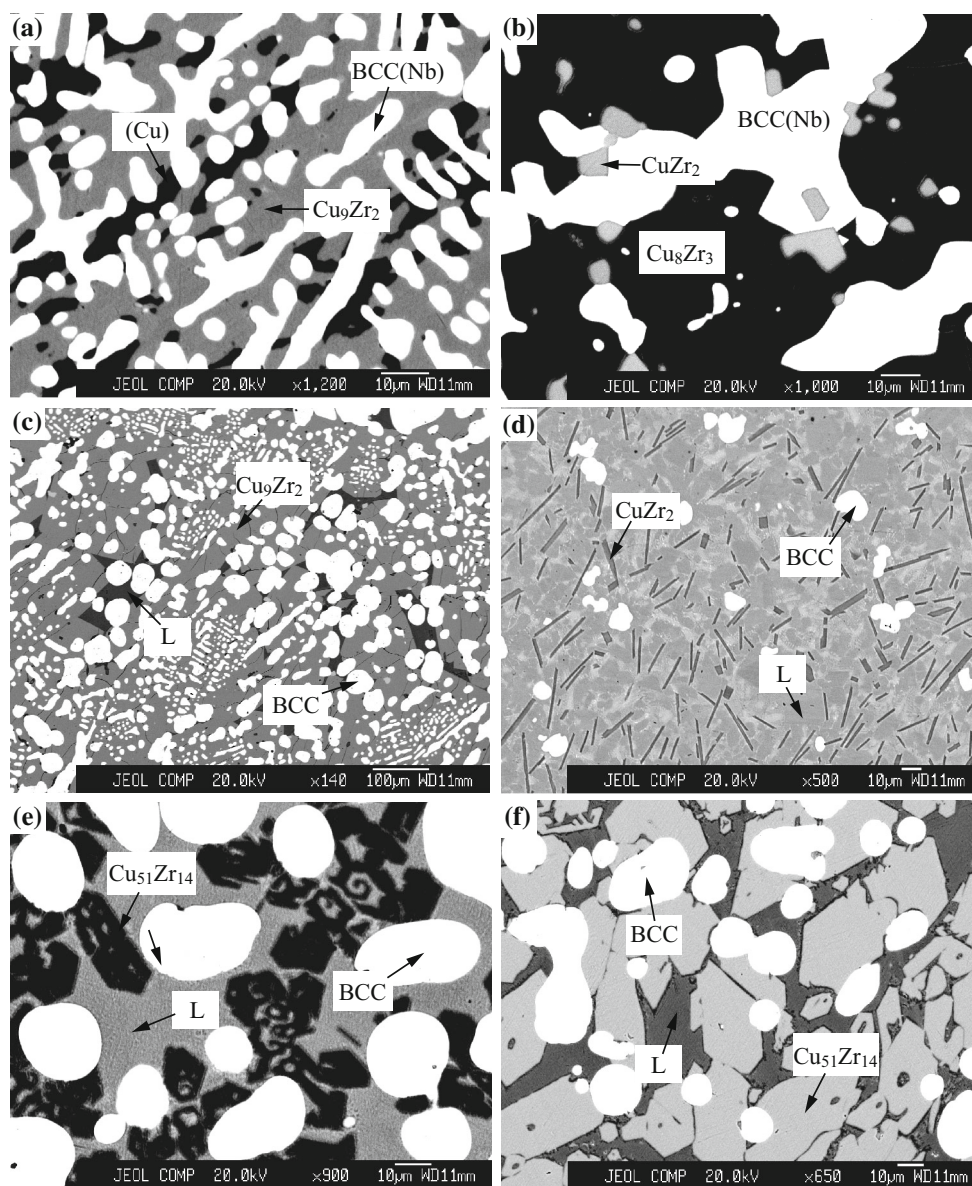
Fig. 2 BSE images of the typical ternary Cu-Nb-Zr alloys: (a) the Cu$_{60}$Nb$_{30}$Zr$_{10}$ (at.%) alloy annealed at 900 °C for 38 days, (b) the Cu$_{50}$Nb$_{30}$Zr$_{20}$ (at.%) alloy annealed at 900 °C for 38 days, (c) the Cu$_{60}$Nb$_{30}$Zr$_{10}$ (at.%) alloy annealed at 1000 °C for 12 h, (d) the Cu$_{35}$Nb$_{10}$Zr$_{55}$ (at.%) alloy annealed at 1000 °C for 8 h, (e) the Cu$_{50}$Nb$_{30}$Zr$_{20}$ (at.%) alloy annealed at 1100 °C for 8 h, and (f) the Cu$_{74}$Nb$_{10}$Zr$_{16}$ (at.%) alloy annealed at 1100 °C for 8 h

observed in the Cu$_{50}$Nb$_{30}$Zr$_{20}$ alloy quenched from 900 °C for 38 days, as indicated in Fig. 2(b). Meanwhile, two three-phase equilibria of (Cu$_9$Zr$_2$ + L + BCC) and (CuZr$_2$ + L + BCC) (L means liquid) were identified in the Cu$_{60}$Nb$_{30}$Zr$_{10}$ and Cu$_{35}$Nb$_{10}$Zr$_{55}$ alloys annealed at 1000 °C, respectively (Fig. 2c, d). The Cu$_{50}$Nb$_{30}$Zr$_{20}$ alloy annealed at 1100 °C for 8 h was found to be located in the three-phase region (Cu$_{51}$Zr$_{14}$ + L + BCC), as illustrated in Fig. 2(e). In the Cu$_{74}$Nb$_{10}$Zr$_{16}$ alloy annealed at 1100 °C for 8 h, three-phase equilibrium of (Cu$_{51}$Zr$_{14}$ + L + BCC) was exhibited in Fig. 2(f). In addition, the solidified microstructures of the as-cast Cu$_{48}$Nb$_{48}$Zr$_4$, Cu$_{46}$Nb$_{46}$Zr$_8$ and Cu$_{46}$Nb$_{46}$Zr$_8$ alloys were found to appear as separated macroscopic morphologies, which were caused by the liquid

phase separation under cooling in the arc furnace. The typical microstructure of the as-cast Cu$_{48}$Nb$_{48}$Zr$_4$ alloy is shown in Fig. 3, where the macroscopic morphology shows an obvious interface between the Cu-rich and Nb-rich phases. Such microstructures are similar with the ones in the Cu-Fe base alloys, as reported in our previous work.[26,27]

3.2 Isothermal Section

The equilibrium compositions of the Cu-Nb-Zr ternary system in the present study at 900, 1000 and 1100 °C determined by EPMA are listed in the Table 1. Based on the experimental data, three isothermal sections at 900, 1000 and 1100 °C were constructed in Fig. 4(a) to (c), respec-

tively. Undetermined three-phase equilibria were shown in dashed lines. No ternary compound was found in these temperature regions.

From Fig. 4(a) to (c), it is seen that there are small solubilities of Nb in the Cu-Zr binary compounds and (Cu)
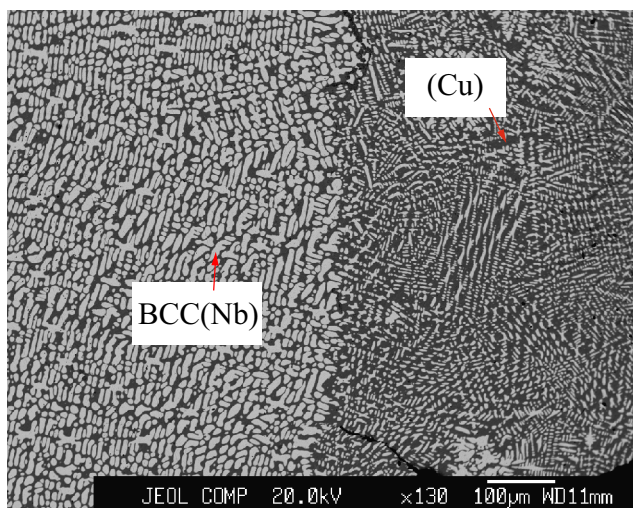

Fig. 3 Separated microscopic morphology of the as-cast $Cu_{48}Nb_{48}Zr_4$ (at.%) alloy

phase. At 900 °C, as indicated in Fig. 4(a), the three-phase region ($CuZr_2$ + BCC(Nb) + BCC(Zr)) was confirmed, which was the result of the spinodal decomposition of BCC in the Nb-Zr system. At the same time, a large three-phase region (Cu_8Zr_3 + $CuZr_2$ + BCC(Nb)) was found at 900 °C, while the other three-phase regions near Cu-Zr side were not determined because of the small range, which were shown in dashed lines. A very large two-phase (L + BCC) region in the Cu-Nb-Zr system existed in the interval 1000 to 1100 °C, as shown in Fig. 4(b) and (c). Liquid regions were both observed at 1000 and 1100 °C, while no liquid region existed at 900 °C.

4. Thermodynamic Calculations

4.1 Thermodynamic Models

In the present work, the thermodynamic models of the phases in the Cu-Nb-Zr system are chosen based on the experimental information of the phase equilibria and the crystal structures. The details of the structures and the used models in the Cu-Nb-Zr ternary system are listed in Table 2. The calculated phase diagrams for binaries Cu-Nb, Cu-Zr and Nb-Zr are shown in Fig. 1. They agree well with the experimental phase equilibrium data as presented in these studies.

Table 1 Equilibrium compositions of the Cu-Nb-Zr ternary alloys determined in the present work

| | | | Phase equilibria | Composition, at.% | | | | | |
| | | | | Phase 1 | | Phase 2 | | Phase 3 | |
Temperature, °C	Alloys, at.%	Annealed time, days	Phase 1/Phase 2/Phase 3	Nb	Zr	Nb	Zr	Nb	Zr
900	$Cu_{10}Nb_{20}Zr_{70}$	38	$CuZr_2$/BCC(Zr)	0.7	67.0	24.3	72.8	…	…
	$Cu_{59}Nb_{20}Zr_{21}$	38	Cu_8Zr_3/$Cu_{51}Zr_{14}$/BCC(Nb)	0.1	27.2	0.1	21.8	94.9	1.3
	$Cu_{60}Nb_{30}Zr_{10}$	38	(Cu)/Cu_9Zr_2/BCC(Nb)	0.01	0.2	0.1	18.0	94.6	0.3
	$Cu_{50}Nb_{30}Zr_{20}$	38	$CuZr_2$/Cu_8Zr_3/BCC(Nb)	2.1	64.9	0.1	27.5	95.9	2.0
	$Cu_{22}Nb_{30}Zr_{48}$	38	$CuZr_2$/BCC(Nb)	1.2	66.8	91.1	8.0	…	…
	$Cu_{10}Nb_{10}Zr_{80}$	38	$CuZr_2$/BCC(Zr)	0.4	67.6	10.3	86.0	…	…
	$Cu_{15}Nb_5Zr_{80}$	38	$CuZr_2$/BCC(Zr)	0.1	66.4	9.2	87.2	…	…
	$Cu_{17}Nb_{30}Zr_{53}$	38	BCC(Nb)/$CuZr_2$/BCC(Zr)	71.4	26.6	0.7	66.0	42.9	54.1
1000	$Cu_{10}Nb_{20}Zr_{70}$	38	$CuZr_2$/BCC	1.5	68.5	24.8	71.3	…	…
	$Cu_{35}Nb_{20}Zr_{45}$	8 h	L/BCC	3.2	47.0	94.8	3.7	…	…
	$Cu_{35}Nb_{10}Zr_{55}$	8 h	$CuZr_2$/L/BCC	5.0	62.2	4.2	50.4	91.1	7.3
	$Cu_{60}Nb_{30}Zr_{10}$	12 h	Cu_9Zr_2/L/BCC	0.1	18.0	0.3	9.8	98.6	0.4
	$Cu_{48}Nb_{48}Zr_4$	12 h	(Cu)/L/BCC	0.1	0.4	0.2	8.2	99.1	0.2
	$Cu_{59}Nb_{20}Zr_{21}$	12 h	$Cu_{51}Zr_{14}$/L/BCC	0.2	21.8	3.2	33.0	96.2	1.5
	$Cu_{22}Nb_{30}Zr_{48}$	38	$CuZr_2$/BCC	2.0	66.1	87.6	11.9	…	…
	$Cu_{17}Nb_{30}Zr_{53}$	38	$CuZr_2$/BCC	1.6	67.8	57.8	41.3	…	…
1100	$Cu_{10}Nb_{20}Zr_{70}$	8 h	L/BCC	5.2	64.2	29.4	67.8	…	…
	$Cu_{50}Nb_{30}Zr_{20}$	8 h	$Cu_{51}Zr_{14}$/L/BCC	0.1	22.6	0.6	28.7	96.7	1.8
	$Cu_{22}Nb_{30}Zr_{48}$	8 h	L/BCC	5.2	59.3	83.8	14.9	…	…
	$Cu_{74}Nb_{10}Zr_{16}$	8 h	$Cu_{51}Zr_{14}$/L/BCC	0.3	20.9	0.4	14.7	96.5	0.4
	$Cu_{35}Nb_{20}Zr_{45}$	8 h	L/BCC	2.4	43.4	95.5	3.0	…	…
	$Cu_{17}Nb_{30}Zr_{53}$	12 h	L/BCC	5.4	60.5	62.9	36.0	…	…
	$Cu_{48}Nb_{48}Zr_4$	12 h	L/BCC	0.1	5.1	97.2	0.3	…	…
	$Cu_{46}Nb_{46}Zr_8$	12 h	L/BCC	0.1	8.9	96.6	0.4	…	…

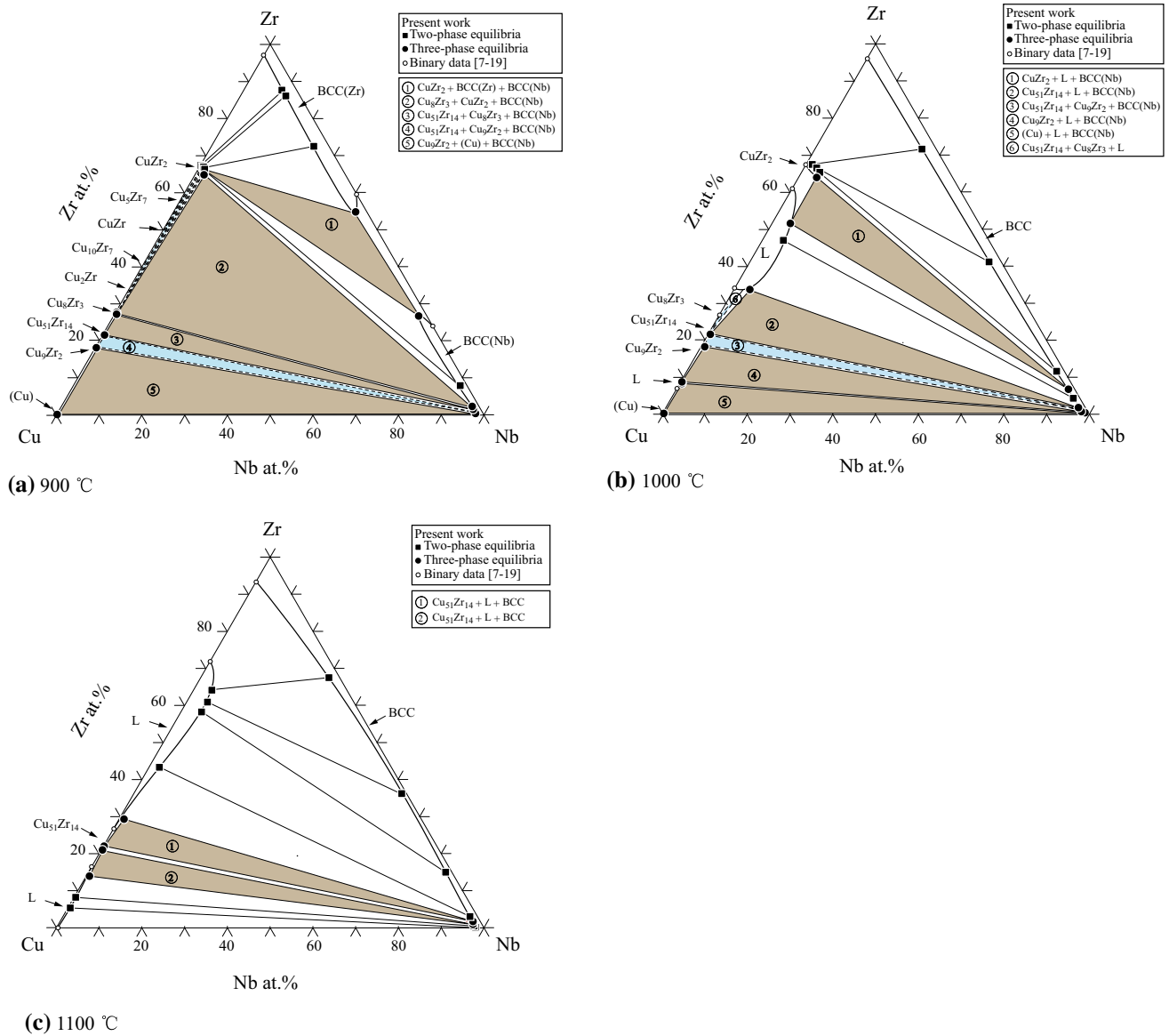**(a)** 900 ℃

(b) 1000 ℃

(c) 1100 ℃

Fig. 4 Experimentally determined isothermal sections of the Cu-Nb-Zr system at (a) 900 °C, (b) 1000 °C and (c) 1100 °C

4.1.1 Solution Phases. The Gibbs free energies of the liquid, bcc, fcc and hcp phases in Cu-Nb-Zr ternary system are described by the sub-regular solution model,[28] as follows:

$$G_m^\phi = {}^0G_{Cu}^\phi x_{Cu} + {}^0G_{Nb}^\phi x_{Nb} + {}^0G_{Zr}^\phi x_{Zr} + RT(x_{Cu}\ln x_{Cu}$$
$$+ x_{Nb}\ln x_{Nb} + x_{Zr}\ln x_{Zr}) + {}^{ex}G^\phi \qquad (Eq\ 1)$$

where G_i^ϕ is the molar Gibbs free energy of pure element i in the phase ϕ phase. R is the gas constant, and T is the absolute temperature. x_i is the fraction of component i, and the term ${}^{ex}G^\phi$ is the excess free energy, which is expressed by the Redlich-Kister polynomials[29] as:

$$^{ex}G^\phi = L_{Cu,Nb}^\phi x_{Cu}x_{Nb} + L_{Cu,Zr}^\phi x_{Cu}x_{Zr} + L_{Nb,Zr}^\phi x_{Nb}x_{Zr}$$
$$+ L_{Cu,Nb,Zr}^\phi x_{Cu}x_{Nb}x_{Zr} \qquad (Eq\ 2)$$

$$L_{i,j}^\phi = {}^0L_{i,j}^\phi + {}^1L_{i,j}^\phi(x_i - x_j) + {}^2L_{i,j}^\phi(x_i - x_j)^2 + {}^3L_{i,j}^\phi(x_i - x_j)^3$$
$$+ \cdots = \sum_{n=0}^{m} {}^nL_{i,j}^\phi(x_i - x_j)^n \qquad (Eq\ 3)$$

$$L_{Cu,Nb,Zr}^\phi = x_{Cu}{}^0L_{Cu,Nb,Zr}^\phi + x_{Nb}{}^1L_{Cu,Nb,Zr}^\phi + x_{Zr}{}^2L_{Cu,Nb,Zr}^\phi$$
$$(Eq\ 4)$$

The binary and the ternary interaction parameters ${}^nL_{i,j}^\phi$ and ${}^nL_{i,j,k}^\phi$ take the following form:

$$^nL_m^\phi = a + bT \qquad (Eq\ 5)$$

where a and b are the coefficients to be optimized in the present work.

Table 2 Crystal structures and the used models of each phase in the the Cu-Nb-Zr ternary system

Phase	Pearson symbol	Prototype	Strukturbericht	Thermodynamic model	Used model
Liquid	…	…	…	(Cu,Nb,Zr)	SSM
FCC(Cu)	$cF4$	Cu	$A1$	(Cu,Nb,Zr)	SSM
BCC(Nb)	$cI2$	W	$A2$	(Cu,Nb,Zr)	SSM
BCC(βZr, βNb)	$cI2$	W	$A2$	(Cu,Nb,Zr)	SSM
Cu_9Zr_2	$tP24$	…	…	$Cu_{0.818}Zr_{0.182}$	SM
$Cu_{51}Zr_{14}$	$hP65$	$Ag_{51}Gd_{14}$	…	$(Cu,Nb)_{0.785}Zr_{0.215}$	SM
Cu_8Zr_3	$oP44$	Cu_8Hf_3	…	$(Cu,Nb)_{0.73}Zr_{0.27}$	SM
Cu_2Zr	$Amm2$	Au_2V	…	$Cu_{0.667}Zr_{0.333}$	SM
$Cu_{10}Zr_7$	$oC68$	$Zi_{10}Zr_7$	…	$Cu_{0.59}Zr_{0.41}$	SM
CuZr	$cP2$	CsCl	$B2$	$Cu_{0.5}Zr_{0.5}$	SM
Cu_5Zr_7	o	…	…	$Cu_{0.416}Zr_{0.584}$	SM
$CuZr_2$	$tI6$	$MoSi_2$	$C11_b$	$Cu_{0.334}(Nb,Zr)_{0.666}$	SM
HCP(αZr)	$hP2$	Mg	$A3$	(Cu,Nb,Zr)	SSM
BCC(βZr)	$cI2$	W	$A2$	(Cu,Nb,Zr)	SSM

SSM: subregular solution model. SM: sublattice model

Table 3 Thermodynamic parameters of the Cu-Nb-Zr system optimized in the present work

Thermodynamic Parameters (J/mol)	References
Liquid phase: (Cu, Nb, Zr)	
$^0L_{Cu,Nb}^{Liq} = +204361.19 - 89.931411T$	[20]
$^1L_{Cu,Nb}^{Liq} = -105148.17 + 57.81653T$	[20]
$^0L_{Nb,Zr}^{Liq} = 10311$	[21]
$^1L_{Nb,Zr}^{Liq} = 6709$	[21]
$^0L_{Cu,Zr}^{Liq} = -140638.632 + 444.1606T$	[22]
$^1L_{Cu,Zr}^{Liq} = -22066.212 + 84.9923T$	[22]
$^2L_{Cu,Zr}^{Liq} = 56633.154 - 307.3817T$	[22]
$^3L_{Cu,Zr}^{Liq} = -22368.721 + 119.5438T$	[22]
$^0L_{Cu,Nb,Zr}^{Liq} = -253110 + 70T$	This work
$^1L_{Cu,Nb,Zr}^{Liq} = 85445 + 35T$	This work
$^2L_{Cu,Nb,Zr}^{Liq} = -177285 + 40T$	This work
BCC phase: (Cu, Nb, Zr)	
$^0L_{Cu,Nb}^{bcc} = 49480.18$	[20]
$^0L_{Nb,Zr}^{bcc} = +15911 + 3.35T$	[21]
$^1L_{Nb,Zr}^{bcc} = +3919 - 1.091T$	[21]
$^0L_{Cu,Zr}^{bcc} = 356.954 - 5.5499T$	[22]
$^0L_{Cu,Nb,Zr}^{bcc} = 58650 - 70T$	This work
$^1L_{Cu,Nb,Zr}^{bcc} = -178650 + 50T$	This work
$^2L_{Cu,Nb,Zr}^{bcc} = -119570 + 90T$	This work
FCC phase: (Cu, Nb, Zr)	
$^0L_{Cu,Nb}^{fcc} = +45699.84 - 5.22785T$	[20]
$^0L_{Cu,Zr}^{fcc} = 8254.852$	[22]
HCP phase: (Cu, Nb, Zr)	
$^0L_{Cu,Nb}^{hcp} = +20000$	[20]
$^0L_{Nb,Zr}^{hcp} = +24411$	[21]
$^0L_{Cu,Zr}^{hcp} = -52576.592 + 70.9696T$	[22]
Cu_9Zr_2 phase: $(Cu)_{0.818}(Zr)_{0.215}$	
$^0G_{Cu:Zr}^{Cu_9Zr_2} = -9410.421 - 0.40907T + 0.818\,^0G_{Cu}^{fcc} + 0.182\,^0G_{Zr}^{hcp}$	[22]
$Cu_{51}Zr_{14}$ phase: $(Cu, Nb)_{0.785}(Zr)_{0.215}$	
$^0G_{Cu:Zr}^{Cu_{51}Zr_{14}} = -10184.262 - 1.0260T + 0.785\,^0G_{Cu}^{fcc} + 0.215\,^0G_{Zr}^{hcp}$	[22]

Table 3 continued

| Thermodynamic Parameters (J/mol)	References
$^{0}G_{Nb:Zr}^{Cu_{51}Zr_{14}} = 10000 + 0.785\,^{0}G_{Nb}^{bcc} + 0.215\,^{0}G_{Zr}^{hcp}$	This work
$^{0}L_{Cu,Nb:Zr}^{Cu_{51}Zr_{14}} = 37595 - 15T$	This work
$Cu_{8}Zr_{3}$ phase: $(Cu, Nb)_{0.727}(Zr)_{0.273}$	
$^{0}G_{Cu:Zr}^{Cu_{8}Zr_{3}} = -11925.337 - 0.43889T + 0.727\,^{0}G_{Cu}^{fcc} + 0.273\,^{0}G_{Zr}^{hcp}$	[22]
$^{0}G_{Nb:Zr}^{Cu_{8}Zr_{3}} = 73190 - 30T + 0.727\,^{0}G_{Nb}^{bcc} + 0.273\,^{0}G_{Zr}^{hcp}$	This work
$^{0}L_{Cu:Nb,Zr}^{Cu_{8}Zr_{3}} = 0$	This work
$Cu_{2}Zr$ phase: $(Cu)_{0.667}(Zr)_{0.333}$	
$^{0}G_{Cu:Zr}^{Cu_{2}Zr} = -11425.463 - 1.4755T + 0.667\,^{0}G_{Cu}^{fcc} + 0.333\,^{0}G_{Zr}^{hcp}$	[22]
$Cu_{10}Zr_{7}$ phase $(Cu)_{0.588}(Zr)_{0.412}$	
$^{0}G_{Cu:Zr}^{Cu_{10}Zr_{7}} = -20463.114 + 5.8825T + 0.588\,^{0}G_{Cu}^{fcc} + 0.412\,^{0}G_{Zr}^{hcp}$	[22]
$CuZr$ phase: $(Cu)_{0.5}(Zr)_{0.5}$	
$^{0}G_{Cu:Zr}^{CuZr} = -14836.032 + 0.8587T + 0.5\,^{0}G_{Cu}^{fcc} + 0.5\,^{0}G_{Zr}^{hcp}$	[22]
$Cu_{5}Zr_{7}$ phase: $(Cu)_{0.416}(Zr)_{0.584}$	
$^{0}G_{Cu:Zr}^{Cu_{5}Zr_{7}} = -15186.254 + 1.8103T + 0.416\,^{0}G_{Cu}^{fcc} + 0.584\,^{0}G_{Zr}^{hcp}$	[22]
$CuZr_{2}$ phase: $(Cu)_{0.334}(Nb,Zr)_{0.666}$	
$^{0}G_{Cu:Zr}^{CuZr_{2}} = -17045.108 + 4.2935T + 0.334\,^{0}G_{Cu}^{fcc} + 0.666\,^{0}G_{Zr}^{hcp}$	[22]
$^{0}G_{Cu:Nb}^{CuZr_{2}} = -86500 + 500T + 0.334\,^{0}G_{Cu}^{fcc} + 0.666\,^{0}G_{Nb}^{bcc}$	This work
$^{0}L_{Cu:Nb,Zr}^{CuZr_{2}} = -10297.5 + 7.5T$	This work
$^{1}L_{Cu:Nb,Zr}^{CuZr_{2}} = 1139200 - 400T$	This work
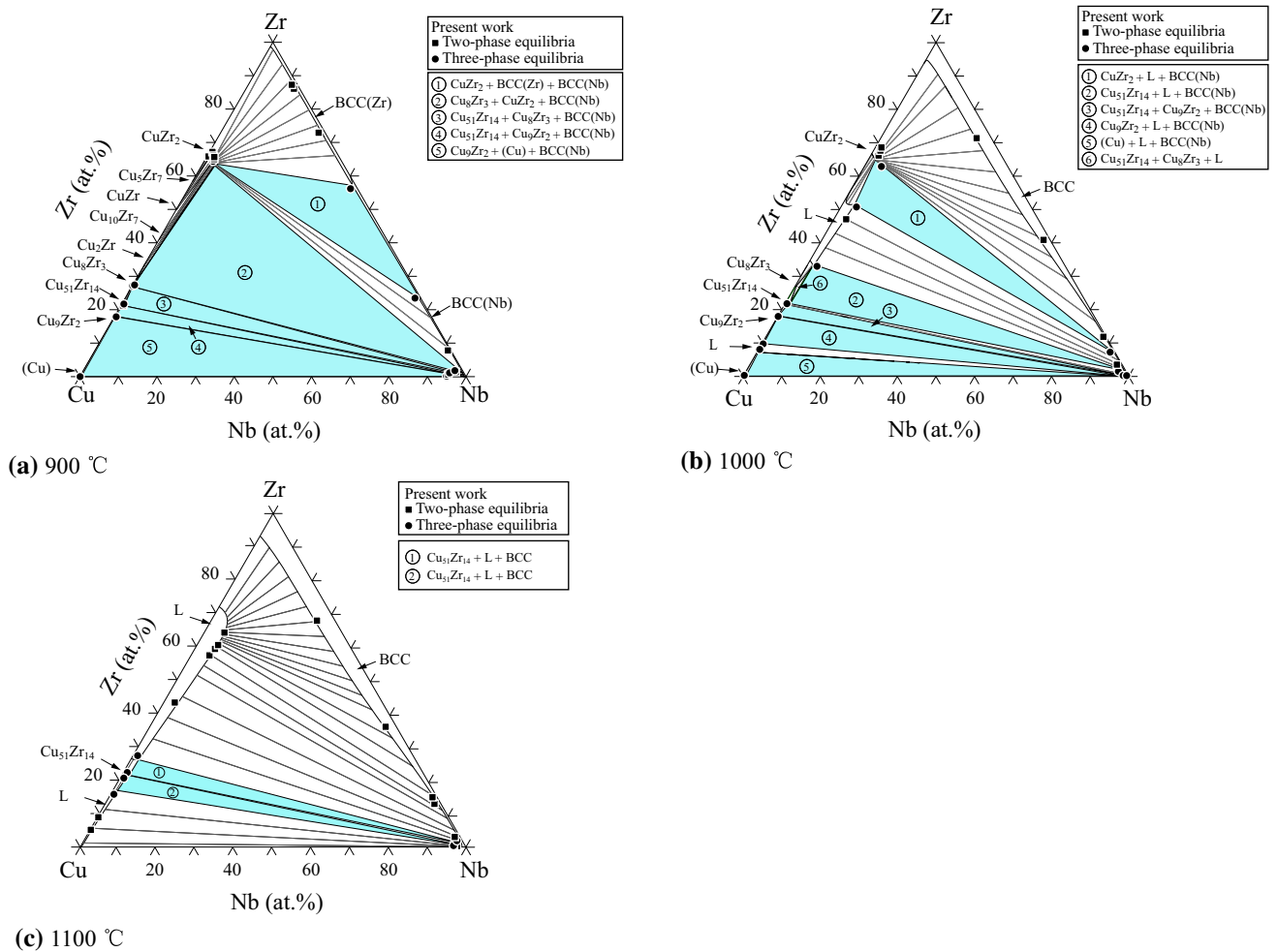
(a) 900 ℃

(b) 1000 ℃

(c) 1100 ℃

Fig. 5 Calculated isothermal sections of the Cu-Nb-Zr system at (a) 900 °C, (b) 1000 °C and (c) 1100 °C comparing with the experimental data
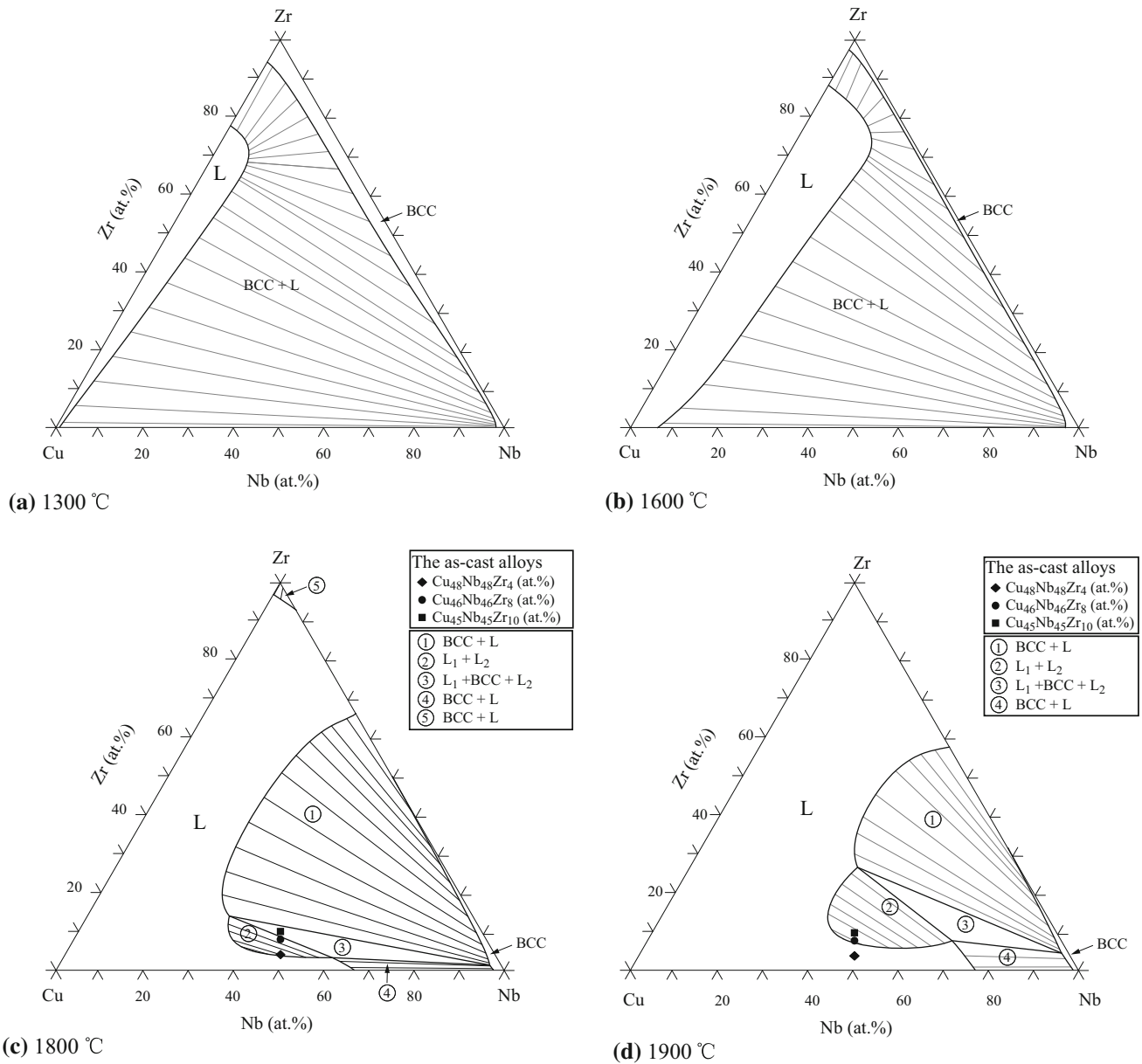
(a) 1300 ℃ (b) 1600 ℃

(c) 1800 ℃ (d) 1900 ℃

Fig. 6 Calculated isothermal sections of the Cu-Nb-Zr system at (a) 1300 °C, (b) 1600 °C, (c) 1800 °C and (d) 1900 °C

4.1.2 Stoichiometric Compounds. The compounds Cu_9Zr_2, Cu_2Zr, $Cu_{10}Zr_7$, CuZr and Cu_5Zr_7 are treated as stoichiometric phases in the Cu-Nb-Zr ternary system because of the small composition extent, while the thermodynamic models are described as $(Cu)_m(Zr)_n$. The Gibbs energy of the Cu_mZr_n phases is expressed as follows:

$$G_m^\phi = m\,^0G_{Cu}^{fcc} + n\,^0G_{Zr}^{hcp} + A + BT \qquad (\text{Eq } 6)$$

where $^0G_{Cu}^{fcc}$ and $^0G_{Zr}^{hcp}$ are the Gibbs energy of the pure elements Cu and Zr, respectively; A and B are parameters to be determined based on the experimental data in the present work.

4.1.3 Binary Phases with Ternary Solubilities. Some phases in the Cu-Nb-Zr system are formed from the terminal binary phases extending into the ternary system. The phase

$CuZr_2$ is extended from the binary phase $CuZr_2$ with partial Zr substituted by Nb. The thermodynamic model of $CuZr_2$ phase is described as $(Cu)_{0.334}(Nb,Zr)_{0.666}$. According to this model, the Gibbs free energy of $CuZr_2$ phase in the Cu-Nb-Zr ternary system is expressed as follows:

$$\begin{aligned}
G_m^{CuZr_2} &= y_{Zr}^{II} G_{Cu:Zr}^{CuZr_2} + y_{Nb}^{II} G_{Cu:Nb}^{CuZr_2} \\
&\quad + 0.666RT\left(y_{Nb}^{II}\ln y_{Nb}^{II} + y_{Zr}^{II}\ln y_{Zr}^{II}\right) \\
&\quad + y_{Nb}^{II} y_{Zr}^{II}\left[\sum_n {}^nL_{Cu:Nb,Zr}\left(y_{Nb}^{II} - y_{Zr}^{II}\right)^n\right]
\end{aligned} \qquad (\text{Eq } 7)$$

The phases $Cu_{51}Zr_{14}$ and Cu_8Zr_3 are extended from the binary phases $Cu_{51}Zr_{14}$ and Cu_8Zr_3 respectively with partial

Cu substituted by Nb. The Gibbs free energy of the phase ϕ ($\phi = Cu_{51}Zr_{14}, Cu_8Zr_3$) with the sublattices $(Cu,Nb)_b$ $(Zr)_c$ ($b + c = 1$) is expressed as follows:

Fig. 7 Calculated miscibility gap of the Cu-Nb system with different Zr additions

$$G_m^\phi = y_{Cu}^I G_{Cu:Zr}^\phi + y_{Nb}^I G_{Nb:Zr}^\phi + bRT\left(y_{Cu}^I \ln y_{Cu}^I + y_{Nb}^I \ln y_{Nb}^I\right)$$
$$+ y_{Cu}^I y_{Nb}^I \left[\sum_n {}^n L_{Cu,Nb:Zr}(y_{Cu}^I - y_{Nb}^I)^n\right]$$

$$\text{(Eq 8)}$$

where y_*^I and y_*^{II} are the site fractions of a certain component located on sublattice *I* and *II*, respectively, and the parameters ${}^0G_{m:n}$ represents the Gibbs free energy of the compound phase when the two sublattices are occupied by element *m* or n_0 The $L_{Cu:Nb,Zr}$ and $L_{Cu,Nb:Zr}$ are the sublattice-type interaction energy between Nb and Zr as well as Cu and Nb when the other sublattice is occupied by the element Cu or Zr. ${}^0G_{m:n}$, $L_{Cu:Nb,Zr}$ and $L_{Cu,Nb:Zr}$ are evaluated in the present work.

4.2 Calculated Results and Discussion

Figure 5(a) to (c) show the calculated isothermal sections of the Cu-Nb-Zr ternary system at 900, 1000 and 1100 °C, compared with the experimental results determined in this work, respectively. On the whole, the calculated results agree reasonably well with the experimental data. The present thermodynamic parameters were carried out on the basis of the experimental data on phase equilibria obtained
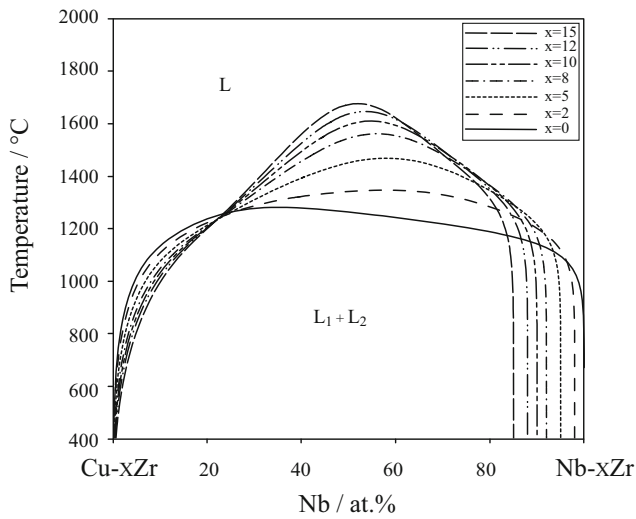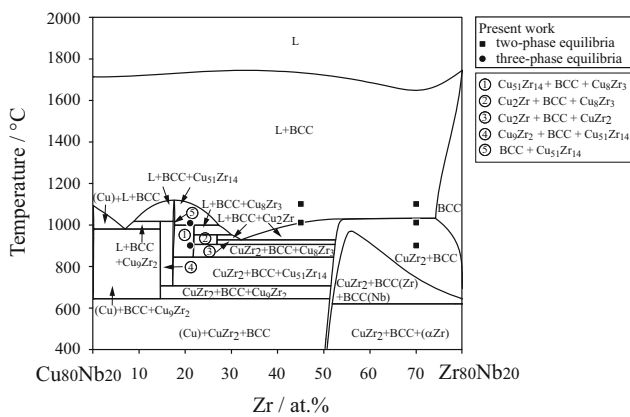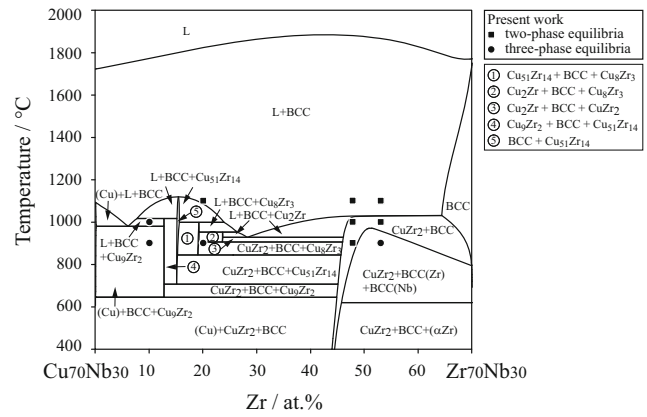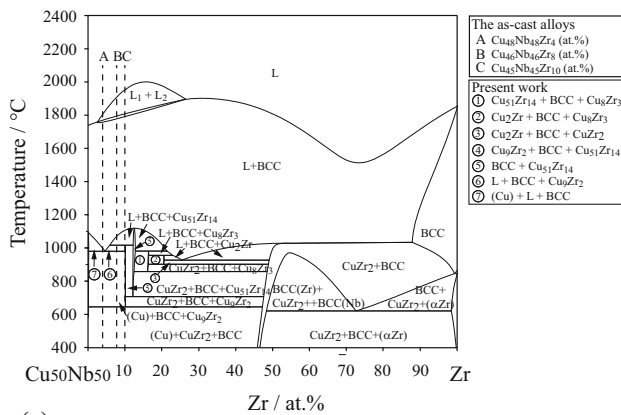

(a)

(b)

(c)

Fig. 8 Calculated vertical sections at (a) 20 at.% Nb, (b) 30 at.% Nb and (c) Cu (at.%):Nb (at.%) = 1:1
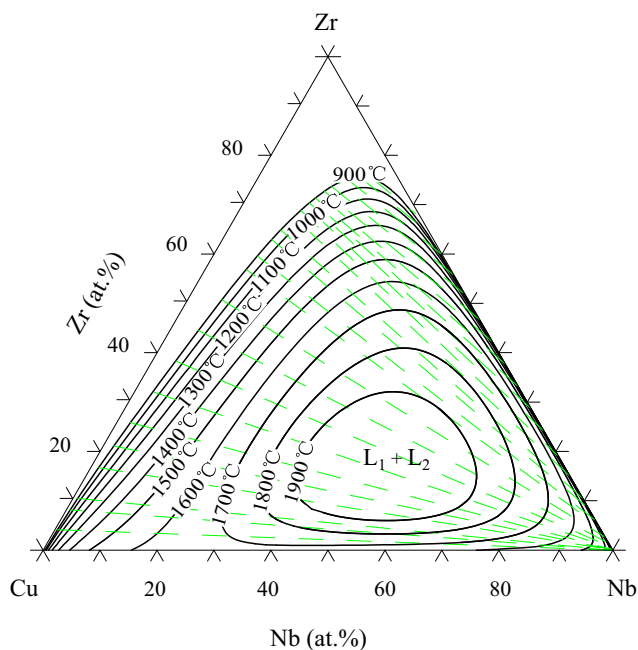
Fig. 9 Calculated liquid miscibility gap of the Cu-Nb-Zr ternary system

in the present work. All the evaluated ternary interaction parameters for each phase in the Cu-Nb-Zr ternary system are listed in Table 3.

The calculated isothermal section at 900 °C is presented in Fig. 5(a). There are five obvious three-phase regions and two bcc phases, which are consistent with the experimental results. Meanwhile, no the liquid phase exists at 900 °C. Figure 5(b) shows six three-phase regions at 1000 °C. Three-phase regions are exhibited in the calculated isothermal section at 1100 °C, as shown in Fig. 5(c).

Figure 6(a) to (d) shows the calculated isothermal sections of the Cu-Nb-Zr system at 1300, 1600, 1800 and 1900 °C. From Fig. 6(a) to (d), it is obviously seen that the liquid region expands with the temperature increasing. As indicated in Fig. 6(c) and (d), the as-cast Cu$_{48}$Nb$_{48}$Zr$_4$ alloy locates inside in the two-phase region (L$_1$ + L$_2$) at 1800 °C, while it exists in the single liquid phase region at 1900 °C. At the same time, the as-cast Cu$_{46}$Nb$_{46}$Zr$_8$ and Cu$_{45}$Nb$_{45}$Zr$_{10}$ alloys both exists in the two-phase region (L$_1$ + L$_2$) at 1800 and 1900 °C. These results imply that the increasing addition of Zr could expand the temperature range of the liquid phase separation. To confirm the results, the calculated liquid miscibility gap of the Cu-Nb system with different additions of Zr is studied, as exhibited in Fig. 7. It clearly indicates that Zr addition can significantly increase the critical temperature of the metastable liquid phase separation in the Cu-Nb system, which shows a good consistency with results in Fig. 6(c) and (d) and experimental data in the present work.

The vertical sections at 20 at.% Nb and 30 at.% Nb are presented in Fig. 8(a) and (b), which are in agreement with the experimental results. In Fig. 8(c), there is a miscibility

gap at high temperatures in the calculated vertical sections diagrams at Cu (at.%):Nb (at.%) = 1:1 of the Cu-Nb-Zr system, which indicates that Zr additions can significantly stabilize the miscibility gap in the Cu-Nb-Zr system. The vertical section at Cu (at.%):Nb (at.%) = 1:1 also shows that the dashed lines representing the as-cast Cu$_{48}$Nb$_{48}$Zr$_4$, Cu$_{46}$Nb$_{46}$Zr$_8$ and Cu$_{45}$Nb$_{45}$Zr$_{10}$ alloys get through the two-phase region (L$_1$ + L$_2$). Figure 9 shows the calculated miscibility gap of liquid phase in the Cu-Nb-Zr ternary system. It can be seen that the tie-lines in the Cu-Nb-Zr system lie from the Nb-rich corner to the Cu-Zr side. The liquid miscibility gap disappears from the middle of the Cu-Nb-Zr triangle.

5. Conclusions

(1) The phase equilibria of the Cu-Nb-Zr system at 900, 1000 and 1100 °C were experimentally determined. No ternary compound was found. A consistent set of thermodynamic parameters have been derived for describing the Gibbs free energies of the solution phases and intermetallic compounds in the Cu-Nb-Zr ternary system, which leads to a good agreement between calculation and experimental data.

(2) The obtained results are beneficial for the designation of Cu-Nb-Zr alloys. The experimental and calculated results show that the solidified microstructures of the as-cast Cu$_{48}$Nb$_{48}$Zr$_4$, Cu$_{46}$Nb$_{46}$Zr$_8$ and Cu$_{45}$Nb$_{45}$Zr$_{10}$ alloys appear as the separated microstructural morphologies, illustrating that the additions of Zr can stabilize the metastable liquid phase separation in the Cu-Nb binary system.

References

1. A. Shikov, V. Pantsyrnyi, A. Vorobieva, N. Khlebova, and A. Silaev, High Strength, High Conductivity Cu-Nb Based Conductors with Nanoscaled Microstructure, *Physica C*, 2001, **354**, p 410-414

2. V.I. Pantsyrny, A.K. Shikov, V.E. Vorobieva, N.E. Khlebova, N.I. Kozlenkova, V.A. Drobishev, I.I. Potapenko, N.A. Beliakov, and M.V. Polikarpova, High Strength, High Conductivity Microcomposite Cu-Nb Wires with Cross Sections in the Range of 0.01-100 mm^2, *Appl. Supercond.*, 2008, **18**, p 616-619

3. W. Głuchowski, J.P. Stobrawa, and Z.M. Rdzawski, Microstructural Characterization of High Strength High Conductivity Cu-Nb Microcomposite Wires, *J. Achiev. Mater. Manuf. Eng.*, 2011, **46**, p 40-49

4. E.N. Popova, V.V. Popov, L.A. Rodionova, E.P. Romanov, S.V. Sudareva, N.E. Hlebova, V.I. Pantsyrny, A.K. Shikov, and A.E. Vorobieva, Effect of Annealing and Doping with Zr on the Structure and Properties of In Situ Cu-Nb Composite Wire, *Scripta Mater.*, 2002, **46**, p 193-198

5. V.A. Frolova, V.V. Bron, and E.M. Savitsky, Strucrure and Superconducting Properties of a Nb-33%Zr Alloy Containing Cu, *Metallovedenie Fiziko-Khimiya i Metall.* 1967, p 74

6. D.L. Kudryavisev and E.M. Tararaeva, the Zr Corner of the Zr-Cu-Nb Phase Diagram, *Fiz. Khim. Splavov Tsirkoniya*, 1968, p 169

7. H. Okamoto and T.B. Massalski, Thermodynamically Improbable Phase Diagrams, *J. Phase Equilibria*, 1991, **12**, p 148-168

8. J.P. Abriata and J.C. Bolcich, The Nb-Zr (Niobium-Zirconium) System, *Bull. Alloy Phase Diagrams*, 1982, **3**, p 33-44

9. M. Hansen and K. Anderko, *Constitution of Binary Alloys*, McGraw-Hill, New York, 1958, p 1023

10. P. Feschotte, D.T. Livey, and O.V. Goldbeck, Plutonium: Physico-Chemical Properties of Its Compounds and Alloys, *At. Energy Rev.*, 1968, **2**, p 66

11. D.L. Douglass, *The Metallurgy of Zirconium*, Supplement, At. Energy Rev., 1971, p 164

12. R. Hultgren, P.D. Desai, D.T. Hawkins, M. Gleiser, K.K. Kelley, and D.D. Wagman, *Selected Values of the Thermodynamic Properties of Binary Alloys*, American Society for Metals, Metals Park, 1973, p 1218

13. O. Kubaschewski-Von, Goldbeck, in Zirconium: Physico-Chemical-Properties of its Compounds and Alloys, *At. Energy Rev.*, 1976, **6**, p 99

14. L. Kaufman and H. Bernstein, *Computer Calculations of Phase Diagrams*, Academic Press, New York, 1970

15. K. Fitzner and O. Kleppa, Thermochemistry of Binary Alloys of Transition Metals: The Me-Ti, Me-Zr, and Me-Hf (Me = Ag, Au) Systems, *Metall. Trans. A*, 1992, **23**, p 997-1003

16. O. Kleppa and S. Watanabe, Thermochemistry of Alloys of Transition Metals: Part III. Copper-Silver, -Titanium, Zirco-nium, and-Hafnium at 1373 K, *Metall. Trans. B*, 1982, **13**, p 391-401

17. M. Turchanin and I. Nikoalenko, Enthalpies of Solution of Titanium, Zirconium, and Hafnium in Liquid Copper, *J. Alloys Compd.*, 1996, **236**, p 236-242

18. K. Yamaguchi, Y. Song, T. Yoshida, and K. Itagaki, Thermodynamic Investigation of the Cu-Zr System, *J. Alloys Compd.*, 2008, **452**, p 73-79

19. Ukr Berezutski, *Khim. Zh.*, 1993, **59**, p 42-44

20. M. Hämäläinen, K. Jääskeläinen, R. Luoma, M. Nuotio, P. Taskinen, and O. Teppo, A Thermodynamic Analysis of the Binary Alloy Systems Cu-Cr, Cu-Nb and Cu-V, *CALPHAD*, 1990, **14**, p 125-137

21. A. Femandez Guillermet, Thermodynamic Analysis of the Stable Phases in the Zr-Nb System and Calculation of the Phase Diagram, *Z. Metallkde*, 1991, **82**, p 478

22. W. Gierlotka, K.C. Zhang, and Y.P. Chang, Thermodynamic Description of the Binary Cu-Zr System, *J. Alloys Compd.*, 2011, **509**, p 8313-8318

23. L. Kaufman and H. Bernstein, *Computer Calculation of Phase Diagram*, Academic Press, New York, 1970

24. N. Saunders and A.P. Miodownik, *CALPHAD (Calculation of Phase Diagrams)-A Comprehensive Guide*, Pergamon Press, Oxford, 1998

25. H. Lukas, S.G. Fries, and B. Sundman, *Computational Thermodynamics—The Calphad Method*, Cambridge University Press, Cambridge, 2007

26. C.P. Wang, X.J. Liu, I. Ohnuma, R. Kainuma, and K. Ishida, Formation of Immiscible Alloy Powders with Egg-Type Microstructure, *Science*, 2002, **297**, p 990-993

27. C.P. Wang, X.J. Liu, Y. Takaku, I. Ohnuma, R. Kainuma, and K. Ishida, Formation pf Core-Type Macroscopic Morphologies in Cu-Fe Base Alloys with Liquid Miscibility Gap, *Metall. Trans. A*, 2004, **35A**, p 1243-1253

28. U.R. Kattner, The Thermodynamic Modeling of Multicomponent Phase Equilibria, *JOM*, 1997, **49**, p 14-19

29. O. Redlich and A.T. Kister, Algebraic Representation of Thermodynamic Properties and the Classification of Solutions, *Ind. Eng. Chem.*, 1948, **40**, p 345-348